Experimental Thermodynamics of Cluster Ions Composed of H_2SO_4 and H_2O. 1. Positive Ions

Karl D. Froyd[†] **and Edward R. Lovejoy***

NOAA Aeronomy Laboratory, 325 Broadway, R/AL2, Boulder, Colorado 80305

Received: December 22, 2002; In Final Form: August 27, 2003

Predictions from gas phase nucleation models are highly sensitive to the thermodynamics of the initial stages of particle growth, where free energies calculated using classical nucleation theory are expected to be the least accurate. There is strong evidence that H_2SO_4 and H_2O are directly involved in atmospheric nucleation. These species are also principal components of atmospheric ions, suggesting that they may play important roles in ion-induced nucleation mechanisms. In part 1 of this work, we measured equilibrium constants for the reactions of H_2O with the cluster ions, $H^+(H_2SO_4)_s(H_2O)_w$, $s \leq 4$ and $w \leq 15$, over a range of temperatures using an ion flow reactor. H_2O bond enthalpies and entropies were derived from van't Hoff analyses, and results for the $H^+(H_2O)_w$ system are in agreement with literature values. Thermodynamics of H_2SO_4 binding in the $H^+(H_2SO_4)_s(H_2O)_w$ cluster ions were also estimated based on comparisons with the $HSO_4^-(H_2SO_4)_s$ system, whose bond enthalpies were measured previously. As clusters grow in size, some thermodynamic trends begin to reflect those for bulk H_2SO_4/H_2O solutions. A stable population of the $H^+(H_2O)_w$ cluster ions is present in the atmosphere, but for typical concentrations, incorporation of the first H_2SO_4 molecule to form $H^+(H_2SO_4)(H_2O)_w$ is thermodynamically unfavorable at 270 K. As a result, significant growth and subsequent nucleation of the $H^+(H_2SO_4)_s(H_2O)_w$ system is not anticipated in the middle or lower troposphere.

Introduction

Gas-phase cluster ions are involved in combustion, heterogeneous processes, nucleation, charge distribution in the Earth's ionosphere and planetary atmospheres, and interstellar matter. Experimental investigations of cluster ion reaction kinetics and thermodynamics, and more recent theoretical treatments of ion−ligand bonding, have yielded a wealth of insight into condensed phases at the molecular level, ion−ligand dynamics, and ion solvation.[1] It has been suggested that observations of gas-phase nucleation in the atmosphere may be initiated by ambient cluster ions.[2] Models of gas phase nucleation require kinetic and thermodynamic data in order to understand particle growth mechanisms and to accurately predict nucleation rates. Although hundreds of ion−molecule reaction rate constants and thermodynamic parameters have been tabulated,[3] several systems potentially important for ion-induced nucleation processes in the atmosphere have not been investigated. Numerous field observations[4] and theoretical treatments[5] suggest that both sulfuric acid and water vapor are directly involved in gas-phase nucleation in the atmosphere. These two species are also principal components of ambient ions in the troposphere and stratosphere,[6] making them ideal precursors to ion-induced nucleation. The purpose of this work is to develop an experimental method to determine thermodynamic quantities ($\Delta G°$, $\Delta H°$, and $\Delta S°$) for the growth and evaporation of cluster ions and to measure these parameters for positive cluster ions composed of H_2SO_4 and H_2O.

Extensive laboratory study of gas-phase cluster ion equilibria began in the 1960s. High-pressure mass spectrometry (HPMS) techniques were developed by Kebarle and co-workers[7−10] to measure cluster ion thermodynamics. The protonated water clusters were one of the first systems to be investigated, and equilibrium measurements of $\Delta G°$, $\Delta H°$, and $\Delta S°$ for the stepwise association of H_2O ligands to form the $H^+(H_2O)_w$ series have been performed by a number of research groups.[8,9,11−15] Thermodynamic parameters for hundreds of cluster ion reactions have now been characterized using both equilibrium and nonequilibrium experimental methods.[3] The $H^+(H_2SO_4)_s(H_2O)_w$ cluster ions were first identified in the laboratory for $s \leq 6$ by Singh et al.[16] using mass spectrometry. Sharp and Futrell[17] later observed the $H^+(H_2SO_4)_s(H_2O)_w$ series up through $s = 20$ using fast atom bombardment of sulfuric acid solutions. Kobara et al.[18] have recently generated $H^+(H_2SO_4)_s(H_2O)_w$, $s \leq 3$ and $w \leq 6$, cluster ions in an electrospray mass spectrometer. Viggiano et al.[19] and Lovejoy[20] measured the reaction kinetics of cluster formation and ligand exchange for several $s = 1$ species. However, the thermodynamics of H_2SO_4-containing positive ions have not been reported.

In this work, equilibrium constants were measured in an ion flow reactor apparatus over a range of temperatures for the reactions of H_2O with positively charged H_2SO_4/H_2O cluster ions

$$H^+(H_2SO_4)_s(H_2O)_{w-1} + H_2O + He \rightleftarrows H^+(H_2SO_4)_s(H_2O)_w + He \quad (1)$$

where the indices s and w refer to the number of H_2SO_4 and H_2O ligands, respectively, in the cluster. A van't Hoff analysis yielded standard reaction enthalpies and entropies, $\Delta H°$ and $\Delta S°$. Extensive laboratory data on the thermodynamics of the protonated water system provides a test case for our experimental measurements. Thermodynamic measurements for the

* To whom correspondence should be addressed. E-mail: nlovejoy@al.noaa.gov.

[†] Also affiliated with the Cooperative Institute for Research in Environmental Sciences, and the Department of Chemistry and Biochemistry at the University of Colorado, Boulder, CO 80309.

10.1021/jp027803o CCC: $25.00
Published on Web 10/29/2003

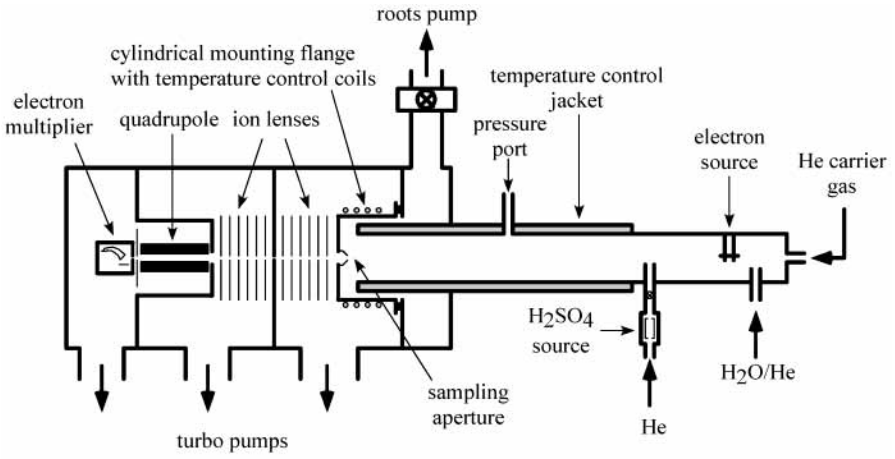

Figure 1. Variable temperature ion flow reactor apparatus.

corresponding negative ion system, $HSO_4^-(H_2SO_4)_s(H_2O)_w$, are described in the accompanying article (part 2)[21] and in our earlier studies.[22]

Experimental Method

Cluster ion equilibrium measurements were performed using a stainless steel, temperature-controlled, low pressure, laminar flow reactor coupled to a quadrupole mass spectrometer (Figure 1). Ions were generated in a 20 cm long × 7.3 cm i.d. tube coupled to the upstream end of the main 113 cm long temperature-controlled flow reactor of the same diameter. The temperature-control jacket begins 13 cm from the upstream end of the main reactor and extends the full length of the reactor, terminating about 4 cm from the sampling aperture. The reaction zone is defined as the distance from the start of the jacket to the sampling aperture, approximately 107 cm. The main helium (99.995%) carrier gas flow, introduced at the upstream end of the ion generation section, ranged from 80 to 175 STP $cm^3\ s^{-1}$ (STP = 760 Torr and 273 K), and represented >90% of the total gas flow during equilibrium measurements. Water vapor was introduced upstream of the ion source. Sulfuric acid vapor was added to the reactor 4 cm upstream of the reaction zone and 22 cm downstream of the ion source. Pressures at the midpoint of the reaction zone, measured using calibrated capacitance manometers, were regulated by a throttle valve on the pump line. Reactor pressures were 1−10 Torr. Mass flow rates of He into the ion reactor, water bubbler, and sulfuric acid source were independently monitored with calibrated commercial flow meters. Gas flow in the reactor was laminar, indicated by a Reynold's numbers of <45. Average linear flow velocities calculated from carrier gas flows and total pressure were 200−6500 cm s^{-1}, yielding cluster ion reaction times of $t = 15-540$ ms. The axial pressure gradient along the reaction zone, ΔP, was typically ≪1% of the reactor pressure, though at $T > 400$ K, the gradient increased to ≈ 2%. Axial pressure gradients were ignored because the resulting changes in thermodynamic values ($\delta\Delta G° < 0.05$ kcal mol^{-1}) are much smaller than the experimental uncertainty.

The ion flow reactor has an operable temperature range of 200−450 K. Gas temperature inside the flow reactor was controlled by circulating hot or cold fluid through the jacket around the reactor. To control the temperature of the ions during sampling, fluid was also circulated through coils of copper tubing soldered to the outside of the large stainless steel cylinder that holds the sampling orifice separating the flow reactor from the first vacuum chamber. The sampling cone and the cylinder were thermally and electrically isolated from the vacuum system. Small thermal losses through the cylinder housing required that the temperature of the fluid inside the copper coils be offset from the fluid in the reactor jacket by up to 8 K to equalize the reactor and sampling temperatures. The gas temperature was measured using a calibrated thermocouple probe protruding from the end of a 1.5 m long × 1/4″ o.d. stainless steel tube inserted down the length of the reactor. The temperature gradient between the end of the flow reactor and the sampling orifice was kept to ≤1 K for all experiments. When operating at temperature extremes (<240 or >400 K), gases would travel up to 40 cm into the reaction zone before the temperature stabilized to within 2 K. Temperature gradients between the center of the reactor and the wall were typically ≤3 K, but gradients of 5 K were observed at high reactor temperature and pressures. Reaction temperature was taken to be that measured at the radial center of the downstream end of the flow reactor. Overall uncertainty in the reaction temperature is estimated to be ±2 K.

Water vapor was introduced into the flow reactor by flowing a He carrier gas through two glass frits at the bottom of a 10 L bubbler filled with 6−8 L of distilled water kept at room temperature. The He/H_2O mixture flowed through a Teflon mesh filter to remove water aerosol, then through a valve that controlled bubbler pressure, and finally into the flow reactor. Helium flow rates through the bubbler ranged from 5 to 55 STP $cm^3\ s^{-1}$ at pressures of 100−1000 Torr. The flow and pressure of H_2O inside the reactor were calculated from helium flows in the reactor and water bubbler, reactor and bubbler pressures, and the saturation vapor pressure of water. The H_2O concentration in the flow reactor was typically $10^{14}-10^{16}$ molecule cm^{-3}. Based on uncertainties in measured pressures and flows, the uncertainty in the calculated [H_2O] values was estimated to be ±10%, which propagates into an uncertainty in $\Delta G°$ for reaction 1 of ±0.1 kcal mol^{-1}.

The sulfuric acid source consisted of a heated (323−343 K) glass sidearm that housed a glass sample boat containing several mL of a solution of H_2SO_4 (impurities <1 ppm) and distilled water. UHP He and distilled water vapor passed over the liquid in the boat, and the H_2SO_4/H_2O/He gas mixture was carried though a Teflon stopcock into a 3/8″ glass tube inserted into the center of the flow reactor. The flow reactor region near the sulfuric acid inlet was heated to ∼350 K to reduce condensation of H_2SO_4 onto the reactor wall. Water vapor was passed over the H_2SO_4 source to prevent dehydration of the H_2SO_4 solution, and thereby lower the vapor pressure of SO_3 over the liquid

($[SO_3]/[H_2SO_4] < 500$).[23] Based on H_2SO_4 and H_2O vapor pressures,[24] the H_2SO_4 mass fraction of the solution was maintained at 80−90 wt %. The sulfuric acid concentration in the flow reactor typically ranged from $[H_2SO_4] \leq 5 \times 10^9$ to 10^{11} molecule cm^{-3}. This estimation does not account for the substantial condensation of H_2SO_4 onto surfaces in the source region and flow reactor, and therefore, it represents an upper limit to the H_2SO_4 concentration in the flow reactor. A more accurate estimation of $[H_2SO_4]$ is given in the Discussion section.

Ions were generated at the upstream end of the flow reactor by electrons emitted at a regulated current of 0.05−1 mA from a heated thoriated iridium filament biased to −100 V. Electrons reacted with ambient He atoms to generate ionic or metastable helium, He^+ and He*. These high energy species reacted rapidly with H_2O molecules to form both positive and negative secondary ions, e.g., H_2O^+, HeH^+, OH^+, and OH^-.[25] The relatively unstable positive ions were then converted to H_3O^+ within a few cm of initial ionization.[26−29] H_3O^+ ions traveled >20 cm (~5 to 50 ms) and were thermalized by $>10^4$ collisions with He before they entered the reaction zone. As gas travels down the flow reactor, growth of cluster ions proceeds through many association and decomposition reactions with H_2SO_4 and H_2O to create the $H^+(H_2SO_4)_s(H_2O)_w$ distribution

$$H^+(H_2SO_4)_s(H_2O)_{w-1} + H_2O \rightarrow H^+(H_2SO_4)_s(H_2O)_w \quad (2)$$

$$H^+(H_2SO_4)_s(H_2O)_w \rightarrow H^+(H_2SO_4)_s(H_2O)_{w-1} + H_2O \quad (3)$$

$$H^+(H_2SO_4)_{s-1}(H_2O)_w + H_2SO_4 \rightarrow H^+(H_2SO_4)_s(H_2O)_w \quad (4)$$

$$H^+(H_2SO_4)_s(H_2O)_w \rightarrow H^+(H_2SO_4)_{s-1}(H_2O)_w + H_2SO_4 \quad (5)$$

Ligand exchange reactions also take place in the reactor

$$H^+(H_2SO_4)_s(H_2O)_w + H_2O \rightarrow H^+(H_2SO_4)_{s-1}(H_2O)_{w+1} + H_2SO_4 \quad (6)$$

$$H^+(H_2SO_4)_s(H_2O)_w + H_2SO_4 \rightarrow H^+(H_2SO_4)_{s+1}(H_2O)_{w-1} + H_2O \quad (7)$$

The proton affinities of H_2O and H_2SO_4 are very similar (PA = 165.0 and 167.2 kcal mol^{-1}),[28] and binary H_2SO_4/H_2O positive ionic clusters are labeled as $H^+(H_2SO_4)_s(H_2O)_w$ because the location of the proton within the cluster ion is not explicitly known. Total ion concentrations in the flow reactor were estimated by calculating the fractional ion flow through the sampling orifice to be $\sim 10^6$ ions cm^{-3} at 3 Torr and 298 K.

The reactor was pumped by a 2000 L s^{-1} Roots pump backed by a large mechanical pump. A small fraction of the gas in the flow reactor was sampled through an orifice into a differentially pumped three chamber vacuum system, where pressures ranged from 10^{-4} to 10^{-7} Torr. The sampling orifice was either a 100 or 250 μm diameter circular aperture laser-drilled through a 3.2 cm diameter × 1.5 cm high conical molybdenum cone located on-axis with the center of the flow reactor. The sampling cone and it's cylindrical mounting flange carried an attractive DC potential of ≤1 V to help direct ion trajectories through the aperture and boost sampling efficiency. Ions with the same polarity as the nose cone were not sampled. As the ions entered the first vacuum chamber, they accelerated toward the stack of attractively biased electrostatic lenses located on-axis with the sampling aperture. All lens potentials were set to <85 V, with the exception of the final lens at the quadrupole entrance, whose potential was typically 100−130 V. Transmission of ions through the lens stack was independent of mass. The ions traveled 21 cm from the sampling aperture through the lenses into the third vacuum chamber where they were mass filtered using a custom built quadrupole with 1/2″ diameter cylindrical rods. The quadrupole filter was controlled with a commercial radio frequency power supply and a computer interface. The quadrupole circuit was resonant at a frequency of 1.2 MHz, corresponding to a maximum peak-to-peak voltage of 2.6 kV, giving an upper mass limit of about 800 amu. The quadrupole operated between constant peak width (Δm) mode and constant resolution ($m/\Delta m$) mode, and therefore, the transmission of ions through the quadrupole was a function of both mass and resolution. Full peak widths at half-maximum intensity (fwhm) were typically 0.8 at 50 amu and 1.5 at 700 amu, corresponding to resolutions of $m/\Delta m = 63$ and 467, respectively. A strong mass discrimination effect was observed with variation of resolution, which significantly altered cluster ion signal ratios. However, as the resolution was lowered, the degree of mass discrimination lessened, and ion peak ratios converged for large ions (500−800 amu) at $m/\Delta m \sim 400$, corresponding to peak widths as large as $\Delta m \sim 2.0$ amu. Measurements were frequently recorded over a range of resolution settings to ensure that no significant mass discrimination occurred.

Ions transmitted through the quadrupole mass filter were detected with a continuous dynode electron multiplier operating in pulse-counting mode. Signals from the multiplier were sent through an amplifier/discriminator, and TTL pulses were counted by the data computer. Raw data were collected by monitoring count rates at different mass-to-charge ratios, corresponding to various cluster ions signals. Software written in our laboratory was used to control data acquisition and record signals generated by the detector. Ion signals (Hz) were collected by performing three to four passes over a set of prescribed cluster ions, where individual ion peak intensities were monitored for a time period of 220−1100 ms per pass. Typical standard deviations of the average signal intensity were 1−4% but were as high as 20% for signals <100 Hz. Background signal levels, defined as the maximum ion signal at a mass where no ions were detected, were ≤10 Hz for an integration time of 220 ms and were generally independent of mass and experimental conditions.

Results

Figure 2 shows mass spectra of the $H^+(H_2SO_4)_s(H_2O)_w$ cluster ion family recorded at 243 K for three different H_2O concentrations. The four distinct groups of ion signals evident in spectrum (b) correspond to, from low to high mass, clusters containing 0, 1, 2, and 3 H_2SO_4 molecules. Each H_2SO_4 group is comprised of multiple spectral peaks due to the equilibration of H_2O over the $H^+(H_2SO_4)_s$ clusters. With an increase in $[H_2O]$, the equilibrium shifts to clusters with more H_2O ligands. For example, the cluster ion with the maximum signal intensity in the $s = 2$ family shifts from $w = 5$ in (a), to $w = 8$ in (b), and finally to $w = 12$ in (c) as the relative humidity is increased from 2% to 61%. The H_2O distributions over each H_2SO_4 series also widen at higher $[H_2O]$. Clusters with more H_2SO_4 molecules can support additional H_2O ligands so that $H^+(H_2SO_4)_s(H_2O)_w$ cluster ion growth in the H_2O coordinate is facilitated by adding H_2SO_4.

The intensity of a peak in the mass spectrum is proportional to the concentration of the ion inside the flow reactor, where the proportionality constant depends on the detection efficiency

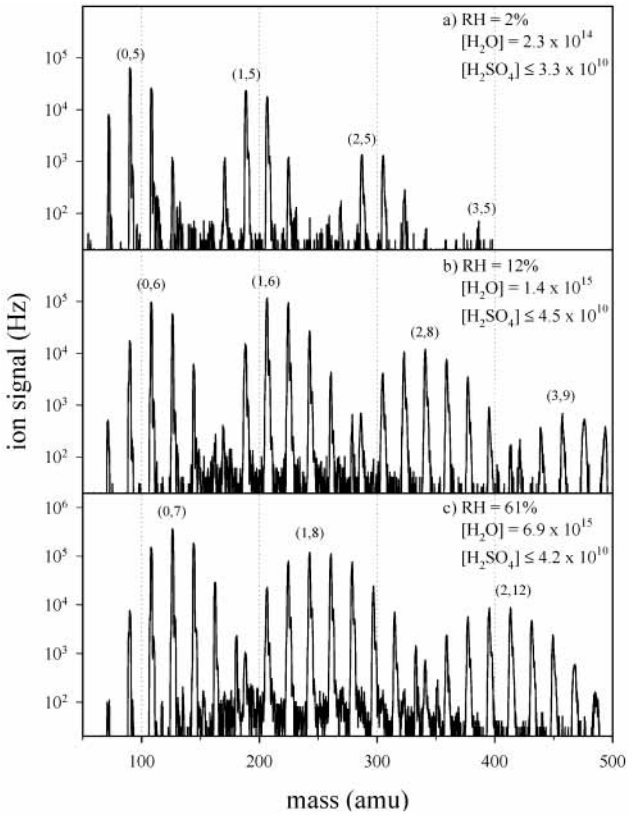

Figure 2. Mass spectra of $H^+(H_2SO_4)_s(H_2O)_w$, $s = 0-3$, recorded at a flow reactor temperature of 243 K. The relative humidity with respect to ice is listed, and H_2O and H_2SO_4 concentrations are given in molecule cm^{-3}. The most intense cluster ion peak in each H_2O envelope is labeled $(s,w) \equiv H^+(H_2SO_4)_s(H_2O)_w$.

of the sampled ion. For the equilibrium reaction 1, the ratio of a product signal, $S_{(s,w)}$, to a reactant signal, $S_{(s,w-1)}$, is equal to the ratio of the product and reactant concentrations inside the flow reactor

$$\frac{S_{(s,w)}}{S_{(s,w-1)}} = \frac{[H^+(H_2SO_4)_s(H_2O)_w]}{[H^+(H_2SO_4)_s(H_2O)_{w-1}]} \quad (8)$$

Because peak ratios are measured for cluster ions 18 amu apart, mass discrimination effects over this range are negligible, and the product and reactant ions are detected with equal efficiency. Peak intensities may be used to define $S_{(s,w)}$ and $S_{(s,w-1)}$ if the intensity measurements for the peaks corresponding to $H^+(H_2SO_4)_s(H_2O)_w$ and $H^+(H_2SO_4)_s(H_2O)_{w-1}$ are recorded at the same relative position on each peak. Equilibrium constants, K_p, for reaction 1 were determined from cluster ion signal intensity ratios and the absolute concentration of water

$$K_p = \frac{S_{(s,w)}}{S_{(s,w-1)}} \frac{1}{P_{H_2O}(\text{atm})} \quad (9)$$

where P_{H_2O} is the gas-phase pressure of H_2O in atm, and the standard Gibbs free energy changes, $\Delta G°$, were calculated. Equilibrium constants were measured at reactor temperatures of 221−434 K and pressures of 0.7−22 Torr. A weighted, linear least-squares fit of the data to the van't Hoff equation

$$\ln K_p = -\Delta H°/RT + \Delta S°/R \quad (10)$$

gives $\Delta H°$ and $\Delta S°$ for each reaction, where points were

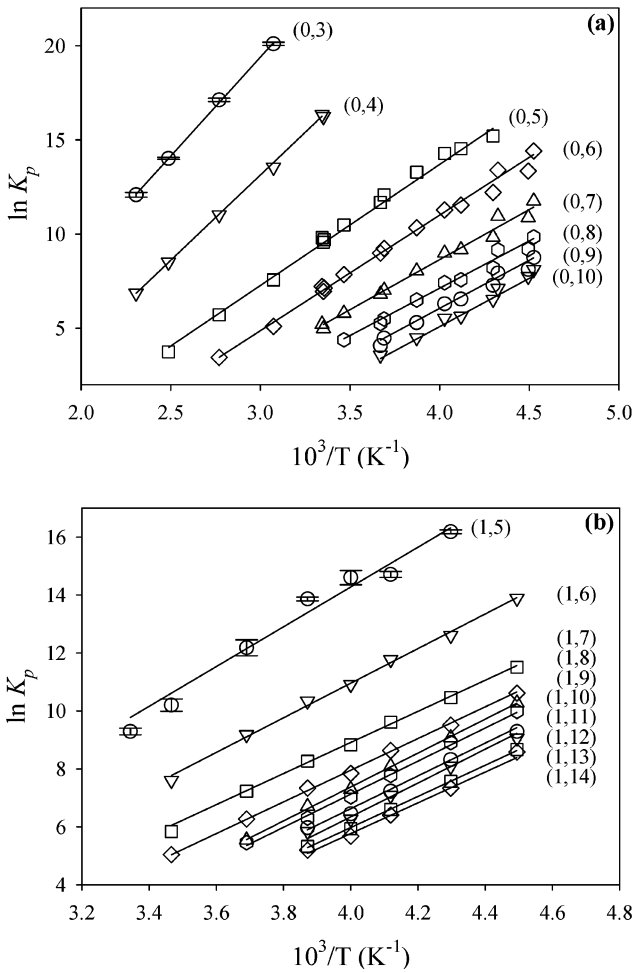

Figure 3. Van't Hoff plots for association of H_2O to form the (a) $H^+(H_2O)_w$, $w = 3-10$, and (b) $H^+(H_2SO_4)(H_2O)_w$, $w = 5-14$, cluster ion series via reaction 1. Points represent averages of multiple experimental measurements, and lines are weighted, linear least-squares fits to the data. Typical error bars shown for (0,3) and (1,5) represent one standard deviation of ln K_p. Product clusters are labeled (s,w).

weighted as the inverse square of the standard deviation of ln K_p. The temperature dependence of $\Delta H°$ and $\Delta S°$ are functions of the heat capacity change for the reaction, $\Delta C_p°$, and eq 10 is only strictly valid over a limited temperature range. By assuming a linear fit to eq 10, using $\Delta C_p°$ values estimated from ab initio calculations of the $HSO_4^-(H_2SO_4)_s(H_2O)_w$ clusters,[21] errors in $\Delta G°$ of $\leq$ 0.1 kcal mol^{-1} are predicted over atmospheric temperatures (200−300 K). Van't Hoff plots for the $H^+(H_2O)_w$ and $H^+(H_2SO_4)(H_2O)_w$ cluster ions are shown in Figure 3. Points are the averages of 2−34 individual measurements of the equilibrium constant for each cluster ion reaction over a range of H_2O concentrations. $\Delta G°$, $\Delta H°$, and $\Delta S°$ values are listed in Table 1. Large 95% confidence intervals of $\Delta S°$ for some clusters (>5 cal mol^{-1} K^{-1}) are a result of the limited accessible temperature range of the measurements, but because measurements were performed over atmospheric temperatures, only small extrapolations are required for determination of $\Delta G°(T)$, $T = 200-300$ K. Propagation of uncertainties in experimental parameters such as flow reactor temperature and H_2O concentration give estimated errors in $\Delta G°$ that are similar to experimental precision uncertainties (typically <0.5 kcal mol^{-1}). However, systematic effects such as mass discrimination or interfering background signals may also contribute to experimental error, and total uncertainties in $\Delta G°$ values are estimated to be on the order of ± 1 kcal mol^{-1}.

TABLE 1: Thermodynamic Results for the Reactions, $H^+(H_2SO_4)_s(H_2O)_{w-1} + H_2 \leftrightarrow OH^+(H_2SO_4)_s(H_2O)_w$ for $s = 0-3$[a]

T	(0,3)	(0,4)	(0,5)	(0,6)	(0,7)	(0,8)	(0,9)	(0,10)	(0,11)
				−6.33[b]	−5.16	−4.32	−3.84	−3.56	
221				0.05[c]	0.06	0.04	0.04	0.02	
				8[d]	10	10	10	2	
				−5.90	−4.81	−4.06	−3.59	−3.43	
223				0.08	0.06	0.05	0.05	0.11	
				12	12	12	12	8	
				−6.15	−5.03	−4.21	−3.64	−3.27	
231				0.04	0.08	0.05	0.04	0.03	
				4	14	14	12	6	
			−7.03	−5.65	−4.55	−3.79	−3.37	−3.02	−2.94
233			0.02	0.05	0.06	0.08	0.05	0.01	0.08
			4	8	8	8	6	4	4
			−7.01	−5.57	−4.43	−3.66	−3.16	−2.72	−2.63
243			0.04	0.05	0.03	0.03	0.10	0.01	0.04
			8	12	12	12	14	6	2
			−7.04	−5.57	−4.43	−3.66	−3.10	−2.73	
248			0.06	0.04	0.04	0.03	0.02	0.03	
			6	14	16	16	10	4	
			−6.82	−5.30	−4.13	−3.33	−2.72	−2.31	−2.15
258			0.16	0.09	0.03	0.07	0.04	0.04	0.05
			6	8	8	6	10	6	4
			−6.50	−4.97	−3.78	−2.96	−2.41		
271			0.16	0.11	0.06	0.11	0.01		
			6	8	8	4	2		
			−6.32	−4.86	−3.69	−2.84	−2.21	−1.94	
273			0.03	0.03	0.04	0.07	0.11	0.03	
			14	16	16	12	6	2	
			−6.01	−4.50	−3.32	−2.52			
289			0.04	0.04	0.02	0.08			
			10	10	10	10			
		−9.62	−5.68	−4.12	−2.95				
298		0.04	0.02	0.05	0.08				
		12	16	16	12				
			−5.74	−4.23					
298			0.13	0.16					
			34	30					
		−9.71	−5.83	−4.29	−3.10				
299		0.03	0.03	0.04	0.07				
		8	16	16	8				
	−13.00	−8.76	−4.89	−3.30					
325	0.06	0.05	0.06	0.04					
	4	26	26	8					
	−12.28	−7.91	−4.10	−2.47					
361	0.06	0.05	0.04	0.04					
	8	20	16	4					
	−11.19	−6.79	−3.00						
402	0.04	0.03	0.04						
	16	16	8						
	−10.41	−5.91							
434	0.11	0.05							
	24	20							
$\Delta H°$	−20.9	−18.0	−12.8	−12.2	−10.6	−10.0	−10.2	−10.2	
σ	0.3	0.1	0.1	0.1	0.1	0.2	0.1	0.1	
95% CI	1.3	0.3	0.1	0.2	0.3	0.5	0.3	0.4	
$\Delta S°$	−24.1	−27.9	−23.8	−26.9	−25.1	−25.8	−28.6	−30.7	
σ	0.8	0.3	0.2	0.3	0.5	0.9	0.4	0.6	
95% CI	3.5	0.8	0.5	0.7	1.0	2.2	1.0	1.5	

T	(1,5)	(1,6)	(1,7)	(1,8)	(1,9)	(1,10)	(1,11)	(1,12)	(1,13)	(1,14)
		−6.14[b]	−5.09	−4.69	−4.54	−4.41	−4.11	−4.01	−3.83	−3.79
223		0.06[c]	0.04	0.07	0.08	0.06	0.06	0.06	0.02	0.03
		6[d]	12	12	12	12	10	10	10	6
	−7.48	−5.83	−4.84	−4.40	−4.19	−4.12	−3.85	−3.74	−3.50	−3.39
233	0.03	0.09	0.06	0.10	0.11	0.05	0.01	0.01	0.00	0.00
	2	6	8	8	8	8	4	4	4	4
	−7.10	−5.68	−4.64	−4.16	−3.90	−3.75	−3.49	−3.42	−3.19	−3.09
243	0.05	0.09	0.04	0.04	0.06	0.04	0.06	0.03	0.04	0.00
	6	12	16	16	14	14	10	8	6	6
	−7.25	−5.42	−4.39	−3.90	−3.63	−3.49	−3.20	−3.11	−2.95	−2.82
R250	0.12	0.12	0.07	0.08	0.07	0.05	0.10	0.03	0.03	0.02
	4	20	20	18	16	12	8	6	4	4
	−7.12	−5.31	−4.24	−3.77	−3.44	−3.23	−3.06	−3.00	−2.73	−2.67

TABLE 1 (Continued)

T	(1,5)	(1,6)	(1,7)	(1,8)	(1,9)	(1,10)	(1,11)	(1,12)	(1,13)	(1,14)
258	0.03	0.12	0.04	0.05	0.05	0.05	0.11	0.07	0.03	0.05
	4	10	16	16	12	12	6	6	6	4
	−6.56	−4.94	−3.89	−3.38	−2.99	−2.94				
271	0.15	0.09	0.09	0.08	0.04	0.05				
	10	18	18	12	8	6				
	−5.85	−4.36	−3.35	−2.89						
289	0.12	0.12	0.11	0.00						
	6	12	10	2						
	−5.52									
299	0.07									
	2									
$\Delta H°$	−13.6	−11.9	−10.7	−10.9	−11.6	−11.3	−11.3	−11.6	−10.7	−10.5
σ	0.2	0.4	0.3	0.2	0.4	0.3	0.6	0.3	0.2	0.1
95% CI	0.6	1.0	0.8	0.4	1.1	0.9	2.0	0.9	0.6	0.3
$\Delta S°$	−26.2	−25.7	−24.9	−27.6	−31.8	−31.2	−31.9	−33.8	−30.8	−30.7
σ	1.0	1.6	1.2	0.5	1.6	1.3	2.7	1.3	0.8	0.4
95% CI	2.5	4.2	3.1	1.4	4.4	3.6	8.4	4.0	2.7	1.3

T	(2,5)	(2,6)	(2,7)	(2,8)	(2,9)	(2,10)	(2,11)	(2,12)	(2,13)	(2,14)	(2,15)	(2,16)
			−5.61[b]	−5.36	−5.07	−4.90	−4.80	−4.62	−4.38	−4.21	−4.01	−4.00
223			0.02[c]	0.01	0.04	0.06	0.08	0.10	0.07	0.09	0.05	0.09
			4[d]	4	8	12	12	12	10	10	10	6
		−6.08	−5.40	−5.04	−4.75	−4.61	−4.40	−4.25	−4.05	−3.90	−3.70	−3.71
233		0.01	0.02	0.03	0.05	0.07	0.10	0.09	0.01	0.01	0.06	0.03
		4	4	4	8	8	8	8	4	4	4	4
	−6.97	−5.84	−5.17	−4.82	−4.49	−4.28	−4.13	−3.95	−3.71	−3.55	−3.39	−3.34
243	0.04	0.07	0.03	0.04	0.02	0.05	0.03	0.07	0.03	0.01	0.02	0.13
	2	8	8	10	16	14	14	10	8	6	6	2
	−6.78	−5.59	−4.90	−4.51	−4.24	−4.07	−3.87	−3.67	−3.45	−3.31	−3.19	
250	0.15	0.11	0.07	0.07	0.04	0.04	0.04	0.06	0.04	0.06	0.06	
	4	8	10	16	16	14	12	10	6	6	4	
	−6.61	−5.45	−4.72	−4.33	−4.00	−3.71	−3.65	−3.51	−3.25	−3.08	−2.97	
258	0.06	0.07	0.05	0.02	0.03	0.15	0.05	0.07	0.05	0.01	0.04	
	4	6	10	10	12	12	12	12	8	8	4	
	−6.16	−5.05	−4.30	−3.92	−3.57	−3.43	−3.22	−3.06				
271	0.08	0.11	0.06	0.06	0.04	0.08	0.02	0.06				
	6	16	14	12	10	8	4	2				
$\Delta H°$	−13.6	−12.1	−11.3	−11.8	−12.0	−11.7	−11.9	−11.6	−11.6	−11.3	−10.5	
σ	0.8	0.4	0.2	0.1	0.2	0.5	0.3	0.5	0.3	0.1	0.4	
95% CI	3.2	1.3	0.6	0.3	0.7	1.3	0.8	1.4	1.0	0.4	1.2	
$\Delta S°$	−27.4	−25.8	−25.6	−28.9	−30.9	−30.5	−31.9	−31.4	−32.5	−32.0	−29.1	
σ	3.0	1.8	1.0	0.5	1.0	1.9	1.1	2.0	1.3	0.5	1.6	
95% CI	12.8	5.7	2.7	1.5	2.8	5.2	3.0	5.6	4.2	1.7	5.1	

T	(3,5)	(3,6)	(3,7)	(3,8)	(3,9)	(3,10)	(3,11)
			−5.70[b]	−5.39	−5.15	−4.96	
233			0.04[c]	0.05	0.04	0.05	
			2[d]	4	4	4	
		−5.88	−5.58	−5.21	−4.94	−4.67	−4.65
243		0.01	0.01	0.03	0.03	0.05	0.09
		2	2	8	6	6	6
		−5.79	−5.28	−4.87	−4.72	−4.43	
250		0.10	0.15	0.05	0.04	0.08	
		4	4	4	2	4	
	−6.38	−5.56	−5.11	−4.73	−4.48	−4.18	−3.95
258	0.04	0.01	0.01	0.05	0.04	0.02	0.04
	2	4	4	4	4	6	2
		−5.17	−4.66	−4.29	−3.93	−3.80	
271		0.01	0.08	0.05	0.08	0.03	
		2	6	8	8	8	
$\Delta H°$		−12.1	−12.3	−12.5	−12.1	−12.1	
σ		0.2	0.3	0.4	0.4	0.3	
95% CI		0.7	0.9	1.3	1.3	1.0	
$\Delta S°$		−25.4	−27.8	−30.2	−29.5	−30.5	
σ		0.6	1.1	1.6	1.7	1.3	
95% CI		2.6	3.5	5.2	5.3	4.0	

[a] Product clusters are labeled (*s*,*w*). Values for each cluster correspond to [b]$\Delta G°$, [c]the standard deviation, and [d]the number of measurements. $\Delta H°$ and $\Delta S°$ values are listed along with standard deviations and 95% confidence intervals for the fits to eq 10. $\Delta G°$ and $\Delta H°$ are given in units of kcal mol^{-1} and $\Delta S°$ is in cal mol^{-1} K^{-1}.

To accurately measure thermodynamic parameters for H_2O ligands in the $H^+(H_2SO_4)_s(H_2O)_w$ cluster ion family, the cluster ions must be in chemical equilibrium with gas-phase H_2O in the flow reactor. The time constant for equilibration via reaction 1 is given by $\tau = 1/(k_1[H_2O] + k_{-1})$, and an upper limit can be written as $\tau \leq 1/(k_1[H_2O])$, where k are the rate coefficients for the forward and reverse reactions in the equilibrium. Second-order rate coefficients for production of $H^+(H_2O)_w$, $w = 2-4$, via reaction 1 range from 3.3×10^{-11} to 7.4×10^{-11} cm^3 molecule^{-1} s^{-1} in 1.5 Torr of helium,[14] and association rate constants for larger cluster ions are probably $10^{-10}-10^{-9}$ cm^3 molecule^{-1} s^{-1} based on kinetic measurements of similar reactions.[29] A typical residence time in the flow reactor of 100 ms and a relatively low H_2O concentration of 1×10^{14} molecule cm^{-3} results in 330 association reaction lifetimes to form the smallest cluster ions. Throughout all experiments, a sufficient number of reaction lifetimes took place in the flow reactor for reaction 1 to attain equilibrium with respect to H_2O. Concurrent to equilibration with H_2O, the cluster ion distribution evolves in the H_2SO_4 coordinate through association and decomposition reactions 4 and 5. Typical H_2SO_4 concentrations of $\sim 10^{10}-10^{11}$ molecule cm^{-3} in the flow reactor correspond to only ~ 1 lifetime for the association reaction 4. Although the time constant for equilibration with H_2SO_4 may instead be dominated by decomposition or ligand exchange reactions 5−7, all cluster ions were probably not in equilibrium with gas-phase H_2SO_4. Because $[H_2O]/[H_2SO_4] > 10^3$, equilibration with H_2O was much faster than redistribution of ions in the H_2SO_4 coordinate via reactions 4−7, and cluster ions maintained equilibrium with H_2O.

To maintain equilibrium, the rate of approach to equilibrium must also exceed the rate of ion loss processes. The dominant ion loss processes were the reaction with the flow reactor walls and with oppositely charged ions. The diffusion-limited wall loss rate constant in a cylindrical reactor with laminar flow is approximately[30,31]

$$k_w = 3.67D/r^2 \qquad (11)$$

where D is the diffusion constant and r is the reactor radius. The ambipolar diffusion constant for $H^+(H_2O)_3$ in He has been measured under similar flow reactor conditions to those in the present work to be 292 Torr cm^2 s^{-1}.[32] In 3 Torr of He, $k_w = 27$ s^{-1} for $H^+(H_2O)_3$, which is more than 100 times slower than the rate constant for cluster ion equilibration with H_2O. The second-order ion−ion recombination rate constant is approximately 10^{-6} cm^3 molecule^{-1} s^{-1},[33] giving first-order recombination rate constants of ~ 1 s^{-1} for concentrations of 10^6 ions cm^{-3}. Overall, the $H^+(H_2SO_4)_s(H_2O)_w$ cluster ion concentration suffered some depletion in the reaction zone due to wall loss and recombination, but equilibrium with H_2O was maintained.

Most of the cluster ion equilibrium measurements were performed using He as the carrier gas because of its chemical inertness, efficiency of thermal equilibration, and low stability of ionic species. As a further test of equilibrium conditions, and to better represent the Earth's atmosphere, one set of measurements was performed using N_2. The total ion signal is significantly reduced when N_2 is passed across the electron filament, and therefore, it was not feasible to use N_2 for all experiments. $\Delta G°$ (298 K) values for formation of $H^+(H_2O)_5$ and $H^+(H_2O)_6$ via reaction 1 using N_2 carrier gas were -5.74 ± 0.13 and -4.23 ± 0.16 kcal mol^{-1} respectively, indistinguishable from the $\Delta G°$ (298−299 K) values using He, -5.75 ± 0.08 and -4.21 ± 0.10 kcal mol^{-1}, where uncertainties are one standard deviation.

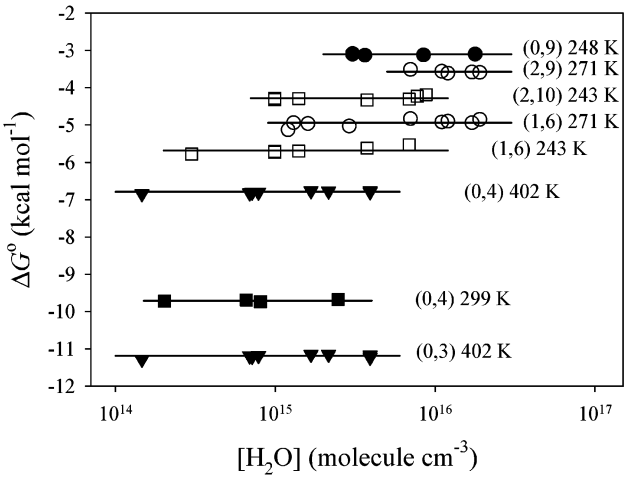

Figure 4. Variation of $\Delta G°$ values for reaction 1 as a function of $[H_2O]$. Representative results for the formation of several $H^+(H_2SO_4)_s(H_2O)_w$ clusters. Lines are average values of $\Delta G°$. Product clusters are labeled (s,w).

Potential complications in the measurement of $\Delta G°$ include nonequilibration, interfering background signals, clustering during ion extraction, and fragmentation due to electric fields. These complications generally lead to a variation in $\Delta G°$ as a function of $[H_2O]$ or other experimental parameters. An interfering background signal underlying a cluster ion peak raises the intensity of that signal, resulting in an inaccurate measurement of $\Delta G°$. The error in $\Delta G°$ increases as the background signal contributes a larger fraction of the total ion signal. Usually, with a change in H_2O concentration, the fractional abundance of the background ion also changes, and $\Delta G°$ will not be constant over a range of $[H_2O]$. An interfering ion, A^+, may also undergo association reactions with H_2O

$$A^+ + n(H_2O) \rightleftarrows A^+(H_2O)_n \qquad (12)$$

In this case, the cluster ion signals of both the product and reactant of reaction 1 are contaminated with background signals, and the measured equilibrium constant would describe two concurrent equilibria, reactions 1 and 12. If the actual equilibrium constants for these two reactions were similar, little variation of $\Delta G°$ over $[H_2O]$ would be observed, and the measured $\Delta G°$ value would be valid for reaction 1. However, because H_2O will not necessarily bind to both A^+ and $H^+(H_2SO_4)_s(H_2O)_{w-1}$ with the same strength, a trend in $\Delta G°$ values would likely be observed over the range of H_2O concentrations. Measured $\Delta G°$ values for the formation of several $H^+(H_2SO_4)_s(H_2O)_w$ cluster ions via reaction 1 are plotted in Figure 4 for a range of flow reactor H_2O concentrations. Where experimentally possible, measurements were conducted over a $[H_2O]$ range of up to 2 orders of magnitude, but clusters located near either end of the observable H_2O distribution could only be detected over more limited concentration range. Measurements were discarded when significant variations in $\Delta G°$ over $[H_2O]$ (>0.3 kcal mol^{-1} per order of magnitude in concentration) were observed. The uniformity of $\Delta G°$ values in Figure 4 also supports the linearity of the flow reactor $[H_2O]$ determination. The water bubbler pressure, helium flow rate through the bubbler, and total reactor pressure and flow rate were adjusted independently throughout the experiments, and consistent $\Delta G°$ results verify that the helium flow through the bubbler was fully saturated with water for all source conditions.

It is critical to the equilibrium measurements that relative cluster ion signals accurately represent the cluster ion distribution

in the flow reactor. Several phenomena may occur during sampling of the gas that can influence the distribution of cluster ions. The mean free path of He molecules was 50−400 μm in the flow reactor, and gas was sampled through a 100 or 250 μm orifice. For these conditions, the sampled gas is in the transition region between effusive and viscous flow. Under noneffusive conditions, carrier gas molecules are cooled due to adiabatic expansion, and the cluster ion distribution may shift to colder temperatures. Under most conditions, no variation of $\Delta G°$ values over reactor pressure or [H_2O] was observed, and $\Delta G°$ values measured with the 100 and 250 μm sampling apertures agreed. During two experiments near room temperature, a sharp trend in $\Delta G°$ for $H^+(H_2SO_4)_s(H_2O)_w$, $s = 0-1$ and $w = 5-7$, was observed for [H_2O] > 10^{15} molecule cm^{-3} when using the larger aperture, and these results were rejected.

Measured $\Delta G°$ values can also be affected by the level of the DC potential on the sampling orifice. Hiraoka and Kebarle[10] reported collision-induced dissociation of sampled $CH_5^+(CH_4)_n$ cluster ions in their mass spectrometer apparatus. At the lowest temperatures, their measured equilibrium constants decreased with pressure for even the most strongly bound $n = 1$ and 2 clusters, and the resulting van't Hoff plots were curved. In the present experiments, sampling cone potentials >1.5 V were also found to fragment cluster ions during sampling, exemplified by a shift of $\Delta G°$ to less negative values. This suggests that cluster ions were translationally heated as they approached the orifice, in contrast to the Hiraoka and Kebarle study, where fragmentation was believed to occur immediately after ion sampling. In the present study, the effective cluster ion heating was more efficient at low reactor pressures, where ions experience fewer thermalizing collisions with the He carrier gas. Enhanced fragmentation observed at high concentrations of H_2O suggests that H_2O molecules are more efficient than He atoms for promoting cluster ion decomposition. The effects of expansive cooling and collision-induced dissociation may offset one another. Although for both effects the cluster ion temperature decreases with increasing pressure, fragmentation can be controlled independently by adjusting the sampling potential, and the presence of either effect can be detected separately.

Discussion

Thermodynamics for H_2O Binding. Results are compared to previous measurements of $\Delta G°$, $\Delta H°$, and $\Delta S°$ to form the protonated water clusters, $H^+(H_2O)_w$, in Table 2 and Figure 5. Van't Hoff lines for the three most complete HPMS studies[9,12,13] and points corresponding to room-temperature measurements from two flowing afterglow studies[14,15] are included. Measurements of $\Delta H°$ and $\Delta S°$ from the current work typically agree with the HPMS studies to within 0.5 kcal mol^{-1} and 2 cal mol^{-1} K^{-1} for $w \geq 4$. The $\Delta H°$ value for the $H^+(H_2O)_3$ cluster is more than 1 kcal mol^{-1} more negative than the two HPMS measurements. The room-temperature flowing afterglow values from Bierbaum et al.[14] for $w = 4$ and 5 are also in agreement with the current study, whereas the $\Delta G°$ result for the $H^+(H_2O)_6$ cluster from Fehsenfeld et al.[15] is ~1 kcal mol^{-1} higher than the present values. Dalleska et al.[34] measured the thermodynamics of the protonated water clusters using collision-induced dissociation. Their $\Delta H°$ values for reaction 1 are within 1.5 kcal mol^{-1} of the mass spectrometry studies for $H^+(H_2O)_w$, $w = 2-6$. Shi et al.[35] determined $\Delta H°$ from H_2O ligand binding energy measurements via ionization of neutral water clusters in a jet expansion. Although Shi's value of $\Delta H°$ to form $H^+(H_2O)_6$ is nearly 4 kcal mol^{-1} more negative than other measurements, values for $w = 7-10$ are within 1.4 kcal mol^{-1} of the currently reported values. The close correspondence of $\Delta H°$ and $\Delta S°$ values to form $H^+(H_2O)_w$ between this work and previous studies in the literature reinforce confidence in the current measurement technique.

TABLE 2: Current and Literature Thermochemical Results for the Reaction, $H^+(H_2O)_{w-1} + H_2O \rightleftarrows H^+(H_2O)_w$[a]

w		this work	ref 9	ref 12	ref 13	ref 14	ref 15	ref 34	ref 35
2	$\Delta H°$		−31.6		−31.8			−32.4	
	$\Delta S°$		−24.3		−24.0				
3	$\Delta H°$	−20.9 (0.3)	−19.5		−19.0			−20.5	
	$\Delta S°$	−24.1 (0.8)	−21.7		−20.9				
4	$\Delta G°$ (296 K)	−9.7 (0.2)				−9.4			
	$\Delta H°$	−18.0 (0.1)	−17.5	−17.9	−17.6			−16.7	
	$\Delta S°$	−27.9 (0.3)	−27.3	−28.4	−27.1				
5	$\Delta G°$ (296 K)	−5.7 (0.1)				−5.5	−4.8		
	$\Delta H°$	−12.8 (0.1)		−12.7	−11.5			−12.7	
	$\Delta S°$	−23.8 (0.2)		−23.4	−19.9				
6	$\Delta H°$	−12.2 (0.1)		−11.6				−12.2	−16.1
	$\Delta S°$	−26.9 (0.3)		−25.0					
7	$\Delta H°$	−10.6 (0.1)		−10.7					−12.0
	$\Delta S°$	−25.1 (0.5)		−26.1					
8	$\Delta H°$	−10.0 (0.2)							−9.8
	$\Delta S°$	−25.8 (0.9)							
9	$\Delta H°$	−10.2 (0.1)							−8.8
	$\Delta S°$	−28.6 (0.4)							
10	$\Delta H°$	−10.2 (0.1)							−9.3
	$\Delta S°$	−30.7 (0.6)							

[a] $\Delta G°$ and $\Delta H°$ are in units of kcal mol^{-1} and $\Delta S°$ are in cal mol^{-1} K^{-1}. Values in parentheses are standard deviations determined from van't Hoff fits.

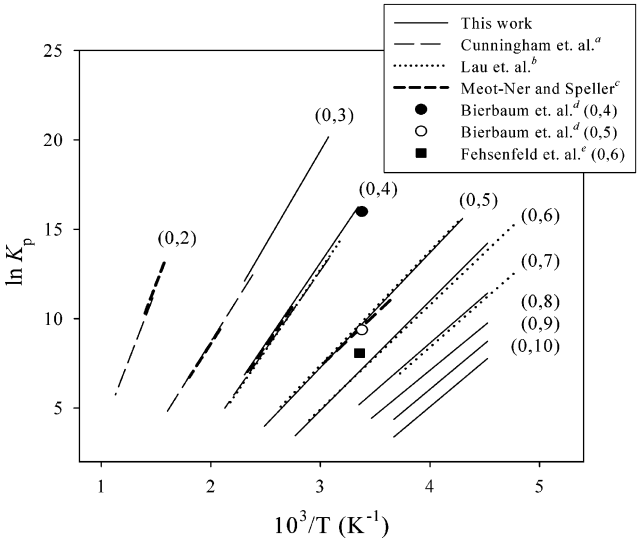

Figure 5. Van't Hoff comparison of experimental measurements of $H^+(H_2O)_{w-1} + H_2O$ $H^+(H_2O)_w$ equilibria. Product clusters are labeled (s,w). [a]Reference 9. [b]Reference 12. [c]Reference 13. [d]Reference 14. [e]-Reference 15.

Plots of association reaction enthalpies and entropies versus the number of H_2O ligands in the $H^+(H_2SO_4)_s(H_2O)_w$ clusters are shown in Figure 6. For the protonated water clusters, $H^+(H_2O)_w$, experimental literature values indicated that the $w = 2$ ligand is quite strongly bound, $\Delta H° \approx -32$ kcal mol^{-1}.[9,13,36] This is consistent with ab initio calculations that predict an $H_2O_5^+$ structure where the proton is shared equally between the two H_2O molecules.[37] Current measurements show that the $w = 3$ and 4 ligands also exhibit firm linkages, $\Delta H° = -20.9$ and −18.0 kcal mol^{-1}, respectively, indicating that these ligands are still strongly influenced by the ion. Ab initio structural

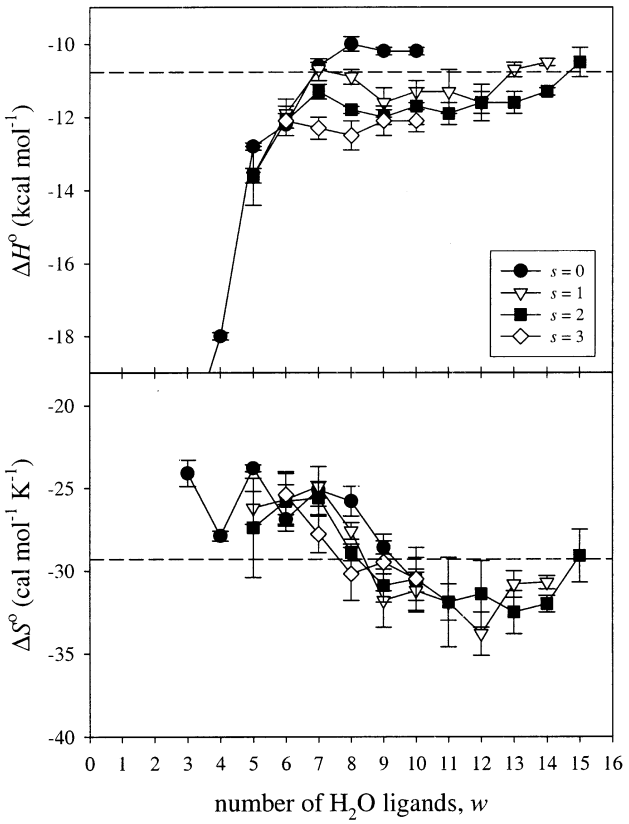

Figure 6. Experimental reaction enthalpy and entropy derived from van't Hoff analyses for the $H^+(H_2SO_4)_s(H_2O)_{w-1} + H_2O \leftrightarrow H^+(H_2SO_4)_s(H_2O)_w$ reactions, $s = 0-3$. Error bars are one standard deviation of the fit parameter and represent precision only. The dashed lines are $\Delta H°_{cond}$(273 K) and $\Delta S°_{cond}$(273 K) for bulk water.

calculations for $H^+(H_2O)_3$ and $H^+(H_2O)_4$ show that H_2O ligands are bound directly to a central H_3O^+ ion, and the $w = 4$ ligand completes the first solvation shell.[38] Binding of H_2O ligands steadily weakens as the core ion is further solvated, and as $H^+(H_2O)_w$ clusters continue to grow to eventually resemble small water droplets, $\Delta H°$ for reaction 1 will converge to the standard molar condensation enthalpy of bulk water, $\Delta H°_{cond}$. Convergence occurs rapidly for the $H^+(H_2O)_w$ series, and by $w = 7$, $\Delta H°$ is within 1 kcal mol^{-1} of $\Delta H°_{cond}$(273 K) = −10.8 kcal mol^{-1}.[26] The $w = 8-10$ ligands are slightly more weakly bound than H_2O molecules in bulk water at 273 K because the H_2O molecules on the outer shell of the cluster are bound by fewer hydrogen bonds than in the bulk.

The H_2SO_4-containing clusters exhibit trends in $\Delta H°$ similar to the $H^+(H_2O)_w$ series. H_2O is bound more strongly at lower w, and $\Delta H°$ values converge toward $\Delta H°_{cond}$ as the number of H_2O ligands increases. Cluster ions containing more H_2SO_4 molecules are somewhat slower to converge. For $w = 5$ and 6, $\Delta H°$ measurements show that H_2O binding is nearly identical regardless of H_2SO_4 content, indicating that H_2SO_4 has little influence on H_2O bonding to these cluster ions. This is in contrast to the trend in a bulk H_2SO_4/H_2O solution where the H_2O vapor pressure decreases somewhat with increasing sulfuric acid mole fraction.[24] The bulk trend becomes evident for larger ($w > 6$) clusters in the $H^+(H_2SO_4)_s(H_2O)_w$ family, where each successive H_2SO_4 molecule provides a small (0.1−1.4 kcal mol^{-1}) stabilizing effect on H_2O ligands. Water association reaction entropy values range from about −24 to −34 cal mol^{-1} K^{-1} for all of the $H^+(H_2SO_4)_s(H_2O)_w$ clusters, independent of H_2SO_4 content, and are comparable to $\Delta S°_{cond}$(273 K) = −29.3 cal mol^{-1} K^{-1} for bulk water.[26] These values are typical of gas phase association reactions, and imply no significant molecular rearrangement or unusually favorable product geometries as a result of H_2O association. These thermodynamic measurements indicate that addition of H_2SO_4 has only a weak effect on the hydrogen bonding network within protonated water clusters, consistent with the similar proton affinities and hydrogen bonding sites of H_2SO_4 and H_2O.

The cluster ions, $H^+(H_2SO_4)_s(H_2O)_w$, $s > 0$ and $w < 4$, were never observed in the mass spectrum. In a previous kinetic study from this laboratory, Lovejoy[20] showed that H_2SO_4 was displaced by H_2O in $H^+(H_2SO_4)(H_2O)_w$, $w = 1-3$, clusters at 330 K

$$H^+(H_2SO_4)(H_2O) + H_2O \rightarrow H^+(H_2O)_2 + H_2SO_4, \quad k = 4 \times 10^{-10}\ \text{cm}^3\ \text{molecule}^{-1}\ \text{s}^{-1} \quad (13)$$

$$H^+(H_2SO_4)(H_2O)_2 + H_2O \rightarrow H^+(H_2O)_3 + H_2SO_4, \quad k = 3 \times 10^{-10}\ \text{cm}^3\ \text{molecule}^{-1}\ \text{s}^{-1} \quad (14)$$

$$H^+(H_2SO_4)(H_2O)_3 + H_2O \rightarrow H^+(H_2O)_4 + H_2SO_4, \quad k = 1 \times 10^{-10}\ \text{cm}^3\ \text{molecule}^{-1}\ \text{s}^{-1} \quad (15)$$

Similarly, kinetic studies of the reverse of reactions 13, 14, and 15 by Viggiano et al.[19] suggest that equilibrium favors the formation of $H^+(H_2O)_w$ for $[H_2O]/[H_2SO_4] = 10$. In the current experiments, the $H^+(H_2SO_4)(H_2O)_4$ cluster ion was observed in equilibrium with $H^+(H_2SO_4)(H_2O)_5$ in the flow reactor, but $H^+(H_2SO_4)(H_2O)_w$, $w = 1-3$, were presumably lost via reactions 13−15. Based on proton-transfer thresholds and the fact that the reaction 13 rate constant is slightly less than the ion−molecule collision rate constant of $k \sim 1 \times 10^{-9}$ cm^3 s^{-1}, Lovejoy determined that reaction 13 is close to ergoneutral ($\Delta G° \approx 0$). The similar rate constants for reactions 14 and 15 suggest that they may also be ergoneutral or slightly endoergic ($\Delta G° > 0$). In the present study, $[H_2O]/[H_2SO_4] > 10^3$, and these reactions were shifted in favor of H_2SO_4 displacement. For most tropospheric conditions ($T > 220$ K, relative humidity > 10%, and $[H_2SO_4] < 10^8$ molecule cm^{-3}), these small $H^+(H_2SO_4)(H_2O)_w$, $w = 1-3$ clusters will not be significantly populated, and thermochemical values for H_2O association to form $w = 2-4$ are not required to predict ambient $H^+(H_2SO_4)(H_2O)_w$ distributions. The $H^+(H_2SO_4)_2(H_2O)_w$, $w < 4$, and $H^+(H_2SO_4)_3(H_2O)_w$, $w < 5$, cluster ions were also not observed in the mass spectra; H_2SO_4 molecules in these clusters were presumably displaced by H_2O.

Investigations of protonated mixtures of water and other strong acids have reported qualitatively similar findings. In a low-pressure ion flow reactor, DNO_3 (PA(HNO_3) = 179.6 kcal mol^{-1})[28] was observed in $D^+(DNO_3)(D_2O)_w$ clusters only for $w \geq 5$,[39] but ligand bond energies were not measured. HCl (PA = 133.1 kcal mol^{-1})[28] has a lower proton affinity than the oxyacids, H_2SO_4 and DNO_3, and it forms fewer hydrogen bonds with solvating H_2O molecules. The $H^+(HCl)(H_2O)_w$ cluster ions have been observed as products of ligand exchange reactions in a Fourier transform ion cyclotron resonance apparatus[40] and also in a thermal system at low temperatures (130−170 K),[41] only for $w \geq 10$.

Estimation of Thermodynamics for H_2SO_4 Binding. No direct thermodynamic measurements exist for H_2SO_4 ligands in $H^+(H_2SO_4)_s(H_2O)_w$ clusters. In the present work, estimations of reaction free energies for the association of H_2SO_4 to form $H^+(H_2SO_4)_s(H_2O)_w$ via reaction 4 were made by modeling the

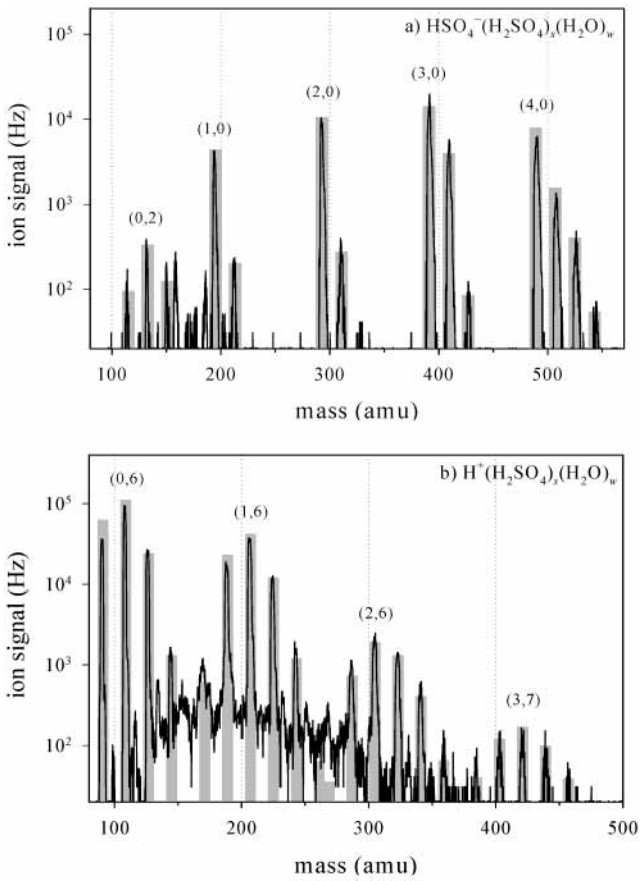

Figure 7. Experimental and simulated mass spectra of (a) $HSO_4^-(H_2SO_4)_s(H_2O)_w$, $s = 0-4$, and (b) $H^+(H_2SO_4)_s(H_2O)_w$, $s = 0-3$, cluster ions at 270 K. The flow reactor pressure was 7.10 Torr, $t = 125$ ms, and $[H_2O] = 5.0 \times 10^{15}$ molecule cm^{-3}. The most intense cluster ion peak in each envelope is labeled (s,w).

growth of cluster ions in the flow reactor using a kinetic simulation under development in our laboratory. Flow reactor H_2SO_4 concentrations were first determined by fitting simulated mass spectra to experimental spectra of the $HSO_4^-(H_2SO_4)_s(H_2O)_w$ cluster ions, whose H_2SO_4 and H_2O thermodynamics are known.[21,22] Simulated $H^+(H_2SO_4)_s(H_2O)$ spectra were then fit to experimental spectra recorded under the same conditions as the negative ions by adjusting $\Delta G^\circ_{s-1,s}$ input values for reaction 4. Ion−molecule rate coefficients for H_2SO_4 association reactions were calculated based on the methods of Su and Chesnavich,[42] and decomposition rate constants were determined from the corresponding equilibrium constants. Ligand exchange reactions 6 and 7 were not included in the model, but evolution of the clusters in the H_2SO_4 coordinate is accurately described by reactions 4 and 5. The ion−ion recombination rate coefficient was set to a constant value of 10^{-6} cm^3 molecule^{-1} s^{-1}.[33] Ion reactions with the walls were not explicitly treated, but this process affects positive and negative ions equally, and estimations of reaction 4 thermodynamics are unaffected by this omission. Ion residence times in the flow reactor were calculated from average flow velocities, $\bar{v}$, and the length of the reaction zone, l_{RZ}

$$t = \frac{l_{RZ}}{1.6\bar{v}} \tag{16}$$

The average velocity of the ions is enhanced by a factor 1.6 relative to the carrier gas because efficient loss of cluster ions at the reactor wall concentrates the ions at the reactor center.[31,43]

TABLE 3: Values of $\Delta G^\circ_{s-1,s}$ for the Reaction $H^+(H_2SO_4)_{s-1}(H_2O)_w + H_2SO_4 \rightarrow H^+(H_2SO_4)_s(H_2O)_w$ Determined from Kinetic Simulations of Ion−Molecule Reactions in the Flow Reactor[a]

	number of H_2SO_4 ligands, s		
number of H_2O ligands, w	1	2	3
1	−25.5[b]		
2	−14.3[b]		
3	−12.5[b]		
4	−10.7	−9.7	−9.8
5	−10.9	−9.4	−9.8
6	−10.9	−9.6	−9.9
7	−11.1	−10.1	−10.3
8	−11.5	−10.7	−10.6
9	−12.0	−11.3	−11.1

[a] All values are for 270 K, and units are kcal mol^{-1}. [b] Estimated values based on measurements by Lovejoy[20] and constrained by $\Delta G^\circ_{w-1,w}$ values via thermochemical reaction cycles.

Figure 7a shows simulated and experimental mass spectra for the $HSO_4^-(H_2SO_4)_s(H_2O)_w$ cluster ion system at 270 K. Simulated H_2SO_4 concentrations yielding the best fits to experimental spectra were consistently ∼20 times lower than $[H_2SO_4]$ estimates calculated from carrier gas flows and pressures and the H_2SO_4 vapor pressure in the source. In the flow reactor, H_2SO_4 is strongly supersaturated relative to the bulk liquid, and the discrepancy between calculated and experimental $[H_2SO_4]$ is due to condensation of H_2SO_4 on the source, inlet, and flow reactor walls. Assuming gas-phase H_2SO_4 condenses on the reactor walls with unit efficiency, and using an estimated diffusion constant for H_2SO_4 in He of 180 Torr cm^2 s^{-1},[44] the concentration of H_2SO_4 would decrease down the length of the flow reactor by a factor of ∼10 at 3 Torr, which roughly agrees with the best fit values for $[H_2SO_4]$. In the simulation, $[H_2SO_4]$ was assumed to be invariant, but this approximation does not greatly affect the estimates of $\Delta G^\circ_{s-1,s}$ for reaction 4.

Figure 7b shows an experimental mass spectrum for the $H^+(H_2SO_4)_s(H_2O)_w$ cluster ion system recorded under the same conditions as the negative ion spectrum in Figure 7a. The simulated spectrum was fit to the experimental spectrum in Figure 7b using measured $\Delta G^\circ_{w-1,w}$ values, $[H_2SO_4] = 1.0 \times 10^{10}$ molecule cm^{-3} from the fit to the spectrum in Figure 7a, and a set of $\Delta G^\circ_{s-1,s}$ values for reaction 4 determined through trial and error. Values for $\Delta G^\circ_{s-1,s}$ were constrained by $\Delta G^\circ_{w-1,w}$ values through thermodynamic cycles. Experiments to estimate $\Delta G^\circ_{s-1,s}$ were performed at 270 K for a range of H_2O concentrations. Under these conditions, $H^+(H_2SO_4)_s(H_2O)_w$ cluster ions grew in the H_2SO_4 coordinate to as large as $s = 3$ and clusters contained from $w = 4-9$ H_2O ligands. Simulations were not performed at lower temperatures because, for the concentrations in the flow reactor, the $HSO_4^-(H_2SO_4)_s(H_2O)_w$ cluster ion decomposition was negligible, and cluster growth was no longer sensitive to H_2SO_4 ligand thermodynamics. Standard Gibbs free energies for H_2SO_4 in the $H^+(H_2SO_4)_s(H_2O)_w$, $w \geq 4$, cluster ions are listed in Table 3. These values are averages of several spectral fitting experiments. The derived set of $\Delta G^\circ_{s-1,s}$ values is consistent with experimental measurements of $\Delta G^\circ_{w-1,w}$ for reaction 1 and also with the estimated thermodynamics of ligand exchange reactions 13−15 by Lovejoy.[20] Using these two constraints, $\Delta G^\circ_{s-1,s}$ values to form $H^+(H_2SO_4)(H_2O)_w$ for $w < 4$ could also be estimated and are listed in Table 3. Because of the indirect nature of the measurement, uncertainties in the derived $\Delta G^\circ_{s-1,s}$(270 K) values are larger than those for directly measured thermodynamic parameters, and are estimated to be ±2 kcal mol^{-1}.

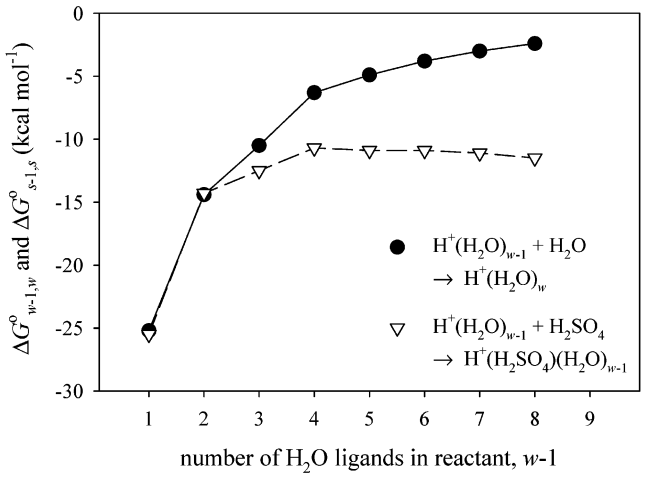

Figure 8. Reaction free energies at 270 K for association of H_2O ($\Delta G^{\circ}_{w-1,w}$) and H_2SO_4 ($\Delta G^{\circ}_{s-1,s}$) to the protonated water clusters, $H^+(H_2O)_{w-1}$.

Gibbs free energies for the competitive uptake of H_2O and H_2SO_4 ligands to the protonated water series are compared in Figure 8. In the smallest clusters, H_2O and H_2SO_4 bond energies are approximately equal. As more water ligands are added to the clusters, the affinity for H_2SO_4 grows, and at $w \geq 4$ H_2SO_4 ligands become more strongly bound than H_2O. The greater stability of H_2SO_4 within the clusters may be partially due to additional hydrogen bonding sites available on the H_2SO_4 molecule, a property that would become advantageous at $w > 3$. In small clusters such as $H^+(H_2SO_4)(H_2O)_4$, a centrally located H_2SO_4 molecule can form direct hydrogen linkages to every H_2O ligand. The proton is likely to be central as well, suggesting that small $H^+(H_2SO_4)(H_2O)_w$ clusters are structured as H_2O ligands surrounding an $H_3SO_4^+$ core ion. The slightly higher proton affinity[28] of H_2SO_4 would also help promote this arrangement. In larger clusters with multiple isomeric geometries, protons within the clusters are probably quite mobile due to the similar proton affinities of H_2SO_4 and H_2O and the fairly homogeneous molecular environment.

In liquid H_2SO_4/H_2O solutions, sulfuric acid exists largely in deprotonated form, as HSO_4^-.[24] It is not thermodynamically favorable for the HSO_4^- ion to exist in the proton-rich environment of small $H^+(H_2SO_4)_s(H_2O)_w$ cluster ions. However, as the clusters grow to where the proton and the H_2SO_4 molecules are well solvated, the molecular environment will begin to resemble that of a bulk solution. Although H_2O ligand bond enthalpies show qualitative agreement with H_2SO_4/H_2O solution thermodynamics, the strong stabilization of H_2SO_4 with increasing H_2O mole fraction in bulk solutions is not evident in the $H^+(H_2SO_4)_s(H_2O)_w$ clusters. ΔG° values for association of H_2SO_4 to these cluster ions are still many kcal mol^{-1} weaker than for bulk solutions with the same composition,[24] suggesting that solvation is incomplete at these sizes. Furthermore, one might expect a large or abrupt reaction entropy change for addition of the final solvating H_2O ligand(s) that enable deprotonation of H_2SO_4. The H_2O reaction entropy data in Figure 6, which show a gradual trend in w and present no obvious distinction between ΔS° curves for $s = 0$ and $s = 1-3$, do not support this hypothesis. Therefore, H_2SO_4 may remain in molecular (or protonated) form within these clusters. H_2SO_4 association reaction entropies and structural calculations would provide more direct insight into the transition toward a bulklike environment.

Atmospheric Implications. Atmospheric ion composition measurements confirm the existence of protonated water clusters.[6] $H^+(H_2O)_w$ cluster ion thermodynamics indicate that water distributions peak at $w = 4-10$ under most tropospheric conditions. However, many gas-phase species, such as CH_3CN, CH_3OH, and NH_3, incorporate into $H^+(H_2O)_w$ clusters,[6] altering their chemistry and shifting the equilibrium H_2O distribution. Although the thermodynamic driving force for incorporation of H_2SO_4 molecules into protonated water clusters is relatively strong, no ambient H_2SO_4-containing positive cluster ions have been identified in the atmosphere. To initiate nucleation of the $H^+(H_2SO_4)_s(H_2O)_w$ cluster ions, several H_2SO_4 molecules may need to be incorporated to provide sufficient cluster stabilization and promote spontaneous growth. However, atmospheric concentrations of H_2O are many orders of magnitude higher than H_2SO_4, and as a result, our thermodynamic data indicate that H_2SO_4 is eliminated from the clusters through the ligand exchange reaction 6. For conditions of $[H_2SO_4] = 10^7$ molecule cm^{-3} at 270 K, $H^+(H_2O)_w$ clusters will outnumber $H^+(H_2SO_4)(H_2O)_w$ at equilibrium by factors of 3300 and 740 for relative humidities of 10% and 90%, respectively. The initial step toward nucleation is highly unfavorable, and therefore, significant concentrations of the $H^+(H_2SO_4)_s(H_2O)_w$ cluster ion family will not form at 270 K. Growth of this cluster ion system may become more thermodynamically favorable at the low temperatures of the upper troposphere.

Conclusions

We have measured the thermodynamics for the stepwise growth of small $H^+(H_2SO_4)_s(H_2O)_w$ cluster ions that are needed to assess the potential for ion-induced nucleation in the atmosphere. Growth of the $H^+(H_2SO_4)_s(H_2O)_w$ cluster ions is initially driven by solvation of the proton by H_2O ligands, forming a stable distribution of $H^+(H_2O)_w$ ions. H_2SO_4 molecules incorporate into these clusters and become more strongly bound than H_2O. However, H_2O ligands do not provide a strong stabilizing affect on H_2SO_4 molecules within the clusters, in contrast to bulk H_2SO_4/H_2O solutions. Ligand bonding trends instead suggest that small ($s \leq 3$) $H^+(H_2SO_4)_s(H_2O)_w$ clusters may have a molecular environment similar to liquid water. In the atmosphere, gas-phase H_2O molecules will drive H_2SO_4 out of the clusters, and under most conditions, nucleation of the $H^+(H_2SO_4)_s(H_2O)_w$ system is probably either thermodynamically unfavorable or negligible compared to competing nucleation mechanisms. Bonding characteristics and the nucleating potential of the $H^+(H_2SO_4)_s(H_2O)_w$ cluster ions are compared to the corresponding negative ion system, $HSO_4^-(H_2SO_4)_s(H_2O)_w$, in the companion paper.[21]

Acknowledgment. The authors acknowledge valuable discussions with J. Curtius and C. J. Howard. This work was conducted at the NOAA Aeronomy Lab while K.F. held a CIRES Graduate Research Fellowship and was supported in part by the NOAA Climate and Global Change Program.

References and Notes

(1) Castleman, A. W. *J. Cluster Sci.* **1990**, *1*, 3. Castleman, A. W.; Keesee, R. G. *Chem. Rev.* **1986**, *86*, 589. Castleman, A. W.; Bowen, K. H. *J. Phys. Chem.* **1996**, *100*, 12911. Castleman, A. W.; Keesee, R. G. *Science* **1988**, *241*, 36. Castleman, A. W.; Wei, S. *Annu. Rev. Phys. Chem.* **1994**, *45*, 685. Kebarle, P. *Int. J. Mass Spectrom.* **2000**, *200*, 313. MacTaylor, R. S.; Castleman, A. W. *J. Atmos. Chem.* **2000**, *36*, 23.

(2) Arnold, F. *Nature* **1980**, *284*, 610. Arnold, F. *Nature* **1982**, *299*, 134. Turco, R. P.; Zhao, J. X.; Yu, F. Q. *Geophys. Res. Lett.* **1998**, *25*, 635. Yu, F. Q.; Turco, R. P. *Geophys. Res. Lett.* **2000**, *27*, 883. Yu, F. Q.; Turco, R. P. *J. Geophys. Res.* **2001**, *106*, 4797.

(3) Keesee, R. G.; Castleman, A. W. *J. Phys. Chem. Ref. Data* **1986**, *15*, 1011. Meot-Ner, M. M.; Lias, S. G. Binding energies between ions and molecules and the thermochemistry of cluster ions. In *NIST Chemistry*

WebBook, NIST Standard Reference Database Number 69, http://webbook.nist.gov; Linstrom, P. J., Mallard, W. G., Eds.; National Institute of Standards and Technology: Gaithersburg, MD, 2001.

(4) Brock, C. A.; Hamill, P.; Wilson, J. C.; Jonsson, H. H.; Chan, K. R. *Science* **1995**, *270*, 1650. Eisele, F. L.; McMurry, P. H. *Phil. Trans. R. Soc. London B* **1997**, *352*, 191. Weber, R. J.; Marti, J. J.; McMurry, P. H.; Eisele, F. L.; Tanner, D. J.; Jefferson, A. *Chem. Eng. Comm.* **1996**, *151*, 53. Weber, R. J.; McMurry, P. H.; Mauldin, L.; Tanner, D. J.; Eisele, F. L.; Clarke, A. D.; Kapustin, V. N. *Geophys. Res. Lett.* **1999**, *26*, 307. Weber, R. J.; Chen, G.; Davis, D. D.; Mauldin, L.; Tanner, D. J.; Eisele, F. L.; Clarke, A. D.; Thorton, D. C.; Bandy, A. R. *J. Geophys. Res.* **2001**, *106*, 24107. Clarke, A. D.; Davis, D. D.; Kapustin, V. N.; Eisele, F. L.; Chen, G.; Paluch, I.; Lenschow, D.; Bandy, A. R.; Thorton, D. C.; Moore, K.; Mauldin, L.; Tanner, D. J.; Litchy, M.; Carroll, M. A.; Collins, J.; Albercook, G. *Science* **1998**, *282*, 89. Clarke, A. D.; Eisele, F. L.; Kapustin, V. N.; Moore, K.; Tanner, D. J.; Mauldin, L.; Litchy, M.; Lienert, B.; Carroll, M. A.; Albercook, G. *J. Geophys. Res.* **1999**, *104*, 5735.

(5) Hamill, P.; Turco, R. P.; Kiang, C. S.; Toon, O. B.; Whitten, R. C. *J. Aerosol Sci.* **1982**, *13*, 561. Jaecker-Voirol, A.; Mirabel, P. *Atmos. Environ.* **1989**, *23*, 2053. Kulmala, M.; Laaksonen, A. *J. Chem. Phys.* **1990**, *93*, 696. Laaksonen, A.; Talanquer, V.; Oxtoby, D. W. *Annu. Rev. Phys. Chem.* **1995**, *46*, 489.

(6) Ferguson, E. E.; Arnold, F. *Acc. Chem. Res.* **1981**, *14*, 327. Arijs, E. D. *Ann. Geophys.* **1983**, *1*, 149. Keesee, R. G.; Castleman, A. W. *J. Geophys. Res.* **1985**, *90*, 5885. Arijs, E. D. *Planet Space Sci.* **1992**, *40*, 255. Viggiano, A. A. *Mass Spect. Rev.* **1993**, *12*, 115.

(7) Kebarle, P.; Godbole, E. *J. Chem. Phys.* **1962**, *36*, 302. Kebarle, P.; Godbole, E. *J. Chem. Phys.* **1963**, *39*, 1131. Hogg, A. M.; Kebarle, P. *J. Chem. Phys.* **1965**, *43*, 449. Hogg, A. M.; Haynes, R. N.; Kebarle, P. *J. Am. Chem. Soc.* **1966**, *88*, 28. Kebarle, P.; Haynes, R. N.; Collins, J. G. *J. Am. Chem. Soc.* **1967**, *89*, 5753. Kebarle, P.; Arshadi, M.; Scarborough, J. *J. Chem. Phys.* **1968**, *49*, 817. Kebarle, P.; Arshadi, M.; Scarborough, J. *J. Chem. Phys.* **1969**, *50*, 1049. Dzidic, I.; Kebarle, P. *J. Phys. Chem.* **1970**, *74*, 1466. Arshadi, M.; Kebarle, P. *J. Phys. Chem.* **1970**, *74*, 1483. Arshadi, M.; Yamdagni, R.; Kebarle, P. *J. Phys. Chem.* **1970**, *74*, 1475.

(8) Kebarle, P.; Hogg, A. M. *J. Chem. Phys.* **1965**, *42*, 798. Kebarle, P.; Searles, S. K.; Zolla, A.; Scarborough, J.; Arshadi, M. *J. Am. Chem. Soc.* **1967**, *89*, 6393. Depaz, M.; Leventhal, J. J.; Friedman, L. *J. Chem. Phys.* **1969**, *51*, 3748. Good, A.; Durden, D. A.; Kebarle, P. *J. Chem. Phys.* **1970**, *52*, 212. Good, A.; Durden, D. A.; Kebarle, P. *J. Chem. Phys.* **1970**, *52*, 222.

(9) Cunningham, A. J.; Payzant, J. D.; Kebarle, P. *J. Am. Chem. Soc.* **1972**, *94*, 7627.

(10) Hiraoka, K.; Kebarle, P. *J. Am. Chem. Soc.* **1975**, *97*, 4179.

(11) Field, F. H. *J. Am. Chem. Soc.* **1969**, *91*, 2827. Beggs, D. P.; Field, F. H. *J. Am. Chem. Soc.* **1971**, *93*, 1567. Beggs, D. P.; Field, F. H. *J. Am. Chem. Soc.* **1971**, *93*, 1576. Bennett, S. L.; Field, F. H. *J. Am. Chem. Soc.* **1972**, *94*, 5186. Meot-Ner, M.; Field, F. H. *J. Am. Chem. Soc.* **1977**, *99*, 998. Yang, X. L.; Castleman, A. W. *J. Am. Chem. Soc.* **1989**, *111*, 6845. Yang, X.; Castleman, A. W. *J. Geophys. Res.* **1991**, *96*, 22573.

(12) Lau, Y. K.; Ikuta, S.; Kebarle, P. *J. Am. Chem. Soc.* **1982**, *104*, 1462.

(13) Meot-Ner, M.; Speller, C. V. *J. Phys. Chem.* **1986**, *90*, 6616.

(14) Bierbaum, V. M.; Golde, M. F.; Kaufman, F. *J. Chem. Phys.* **1976**, *65*, 2715.

(15) Fehsenfeld, F. C.; Mosesman, M.; Ferguson, E. E. *J. Chem. Phys.* **1971**, *55*, 2120.

(16) Singh, J. J.; Smith, A. C.; Yue, G. K. *J. Aerosol Sci.* **1982**, *13*, 285.

(17) Sharp, T. R.; Futrell, J. H. *Int. J. Mass Spectrom. Ion Process.* **1989**, *90*, 39.

(18) Kobara, H.; Wakisaka, A.; Takeuchi, K.; Ibusuki, T. *J. Phys. Chem. A* **2002**, *106*, 4779.

(19) Viggiano, A. A.; Perry, R. A.; Albritton, D. L.; Ferguson, E. E.; Fehsenfeld, F. C. *J. Geophys. Res.* **1980**, *85*, 4551.

(20) Lovejoy, E. R. *Int. J. Mass Spectrom.* **1999**, *191*, 231.

(21) Froyd, K. D.; Lovejoy, E. R. *J. Phys. Chem. A* **2003**, *107*, 9812.

(22) Curtius, J.; Froyd, K. D.; Lovejoy, E. R. *J. Phys. Chem. A* **2001**, *105*, 10867. Lovejoy, E. R.; Curtius, J. *J. Phys. Chem. A* **2001**, *105*, 10874.

(23) Perry, R. H.; Green, D. W.; Maloney, J. O. *Perry's Chemical Engineers' Handbook*, 7th ed.; McGraw-Hill: New York, 1997.

(24) Clegg, S. L.; Brimblecombe, P.; Wexler, A. S. *J. Phys. Chem.* **1998**, *102*, 2A, 2137.

(25) Bartmess, J. E. Negative Ion Energetics Data. In *NIST Chemistry WebBook, NIST Standard Reference Database Number 69*; Linstrom, P. J., Mallard, W. G., Eds.; National Institute of Standards and Technology: Gaithersburg MD, 2001; Vol. NIST Standard Reference Database Number 69. Howard, C. J.; Rundle, H. W.; Kaufman, F. *J. Chem. Phys.* **1970**, *53*, 3745. Bolden, R. C.; Twiddy, N. D. *Discuss. Faraday Soc.* **1972**, *53*, 192.

(26) Chase, M. W., Jr. *J. Phys. Chem. Ref. Data* **1998**, *Monograph 9*, 1.

(27) Cox, J. D.; Wagman, D. D.; Medvedev, V. A. *CODATA Key Values for Thermodynamics*; Hemisphere Publishing Corp.: New York, 1984. Lias, S. G. Ionization Energy Evaluation. In *NIST Chemistry WebBook, NIST Standard Reference Database Number 69, http://webbook.nist.gov*; Mallard, W. G., Ed.; National Institute of Standards and Technology: Gaithersburg MD, 2001; Vol. NIST Standard Reference Database Number 69.

(28) Hunter, E. P.; Lias, S. G. *J. Phys. Chem. Ref. Data* **1998**, *27*, 413.

(29) Ikezoe, Y.; Matsuoka, S.; Takebe, M.; Viggiano, A. A. *Gas-Phase Ion−Molecule Reaction Rate Constants Through 1986*; Ion Reaction Research Group of the Mass Spectroscopy Society of Japan: Tokyo, 1987.

(30) Bolden, R. C.; Hemsworth, R. S.; Shaw, M. J.; Twiddy, N. D. *J. Phys. B* **1970**, *3*, 45. Huggins, R. W.; Cahn, J. H.; Julius, H. *J. Appl. Phys.* **1967**, *38*, 180.

(31) Farragher, A. L. *Trans. Faraday Soc.* **1970**, *66*, 1411.

(32) Dotan, I.; Linderger, W.; Albritton, D. L. *J. Chem. Phys.* **1977**, *37*, 5968.

(33) Bates, D. R. *Planet Space Sci.* **1982**, *30*, 1275. Bates, D. R. *Adv. At. Mol. Phys.* **1985**, *20*, 1.

(34) Dalleska, N. F.; Honma, K.; Armentrout, P. B. *J. Am. Chem. Soc.* **1993**, *115*, 12125.

(35) Shi, Z.; Ford, J. V.; Wei, S.; Castleman, A. W. *J. Chem. Phys.* **1993**, *99*, 8009.

(36) Meotner, M.; Field, F. H. *J. Am. Chem. Soc.* **1977**, *99*, 998.

(37) Auer, A. A.; Helgaker, T.; Klopper, W. *Phys. Chem. Chem. Phys.* **2000**, *2*, 2235. Valeev, E. F.; Schaefer, H. F. *J. Chem. Phys.* **1998**, *108*, 7197.

(38) Lee, E. P. F.; Dyke, J. M. *Molec. Phys.* **1991**, *73*, 375. Cheng, H.-P. *J. Phys. Chem. A* **1998**, *102*, 6201.

(39) Zhang, X.; Mereand, E. L.; Castleman, A. W. *J. Phys. Chem.* **1994**, *98*, 3554.

(40) Schindler, T.; Berg, C.; Niedner-Schatteburg, G.; Bondybey, V. E. *Chem. Phys. Lett.* **1994**, *229*, 57.

(41) MacTaylor, R. S.; Gilligan, J. J.; Moody, D. J.; Castleman, A. W. *J. Phys. Chem.* **1999**, *103*, 4196.

(42) Su, T.; Chesnavich, W. J. *J. Chem. Phys.* **1982**, *76*, 5183. Su, T. *J. Chem. Phys.* **1985**, *82*, 2164.

(43) Howard, C. J. *J. Phys. Chem.* **1979**, *83*, 3.

(44) Poschl, U.; Canagarantna, M.; Jayne, J. T.; Molina, L. T.; Worsnop, D. R.; Kolb, C. E.; Molina, M. J. *J. Phys. Chem. A* **1998**, *102*, 10082.